*Article*

# Syntheses of Nanostructured Magnesium Carbonate Powders with Mesoporous Structures from Carbon Dioxide

Fernando J. Rodríguez-Macías [1,2] , José E. Ortiz-Castillo [1] , Erika López-Lara [1] , Alejandro J. García-Cuéllar [1] , José L. López-Salinas [1] , César A. García-Pérez [1] , Orlando Castilleja-Escobedo [1] and Yadira I. Vega-Cantú [1,2,*]

[1] Tecnologico de Monterrey, Escuela de Ingeniería y Ciencias, Ave. Eugenio Garza Sada 2501, Monterrey 64849, N.L., Mexico; fernando.jrm@tec.mx (F.J.R.-M.); A00815643@itesm.mx (J.E.O.-C.); erika.lopez.laraa@gmail.com (E.L.-L.); ajgarcia@tec.mx (A.J.G.-C.); jllopezs@tec.mx (J.L.L.-S.); cesar.garcia@uaem.mx (C.A.G.-P.); A00826734@itesm.mx (O.C.-E.)

[2] Pós-Graduação em Ciência de Materiais, Universidade Federal de Pernambuco, Av. Prof. Moraes Rego 1235, Cidade Universitária, Recife 50.670-901, PE, Brazil

[*] Correspondence: yadira.vega@tec.mx

**Abstract:** In this work, we present the results of two synthesis approaches for mesoporous magnesium carbonates, that result in mineralization of carbon dioxide, producing carbonate materials without the use of cosolvents, which makes them more environmentally friendly. In one of our synthesis methods, we found that we could obtain nonequilibrium crystal structures, with acicular crystals branching bidirectionally from a denser core. Both Raman spectroscopy and X-ray diffraction showed these crystals to be a mixture of sulfate and hydrated carbonates. We attribute the nonequilibrium morphology to coprecipitation of two salts and short synthesis time (25 min). Other aqueous synthesis conditions produced mixtures of carbonates with different morphologies, which changed depending on drying temperature (40 or 100 °C). In addition to aqueous solution, we used supercritical carbon dioxide for synthesis, producing a hydrated magnesium carbonate, with a nesquehonite structure, according to X-ray diffraction. This second material has smaller pores (1.01 nm) and high surface area. Due to their high surface area, these materials could be used for adsorbents and capillary transport, in addition to their potential use for carbon capture and sequestration.

**Keywords:** porous materials; supercritical carbon dioxide; magnesium carbonate; carbon sequestration

## 1. Introduction

Magnesium carbonates are some of several minerals proposed for "carbon mineralization", one of several approaches to Carbon Capture and Sequestration (CCS) [1]. In situ mineral carbonation is one of the options, but the need for transport to suitable geological sites and other factors make it costly, ex situ mineral carbonation, precipitating magnesium carbonates from solutions containing magnesium ions is another option [2]. Magnesium carbonates exist in different structures with different thermodynamic stability and different degrees of hydration. In general, all magnesium carbonates are of interest in CCS since they have stable and long-lasting forms [3], the most attractive one for CCS is $MgCO_3$, which has a 1:1 molar ratio of magnesium to $CO_2$, but the hydrated forms are favored during precipitation [4]. This makes the study of the precipitation of magnesium carbonates an important field of study. Even if the most desirable forms of anhydrous $MgCO_3$ were not obtained, hydrated magnesium carbonates such as nesquehonite ($MgCO_3·3H_2O$) have been reported to be useful for construction materials [5], a potential application that may sequester carbon for long periods of time.

The synthesis of magnesium carbonates by mineral carbonation (i.e., formation of stable carbonates with minerals) has been studied widely for CCS [2].

Magnesium carbonate is a valuable product by itself, with a price of USD 100–1000/t, depending on purity, which could offset the cost of carbon capture by ex situ mineralization,

estimated to be USD 50–300 per $tCO_2$ sequestered [1]. An option to make magnesium carbonates more valuable would be to create a mesoporous (pore diameters of 2–50 nm) material [6]. The applications of nanostructured mesoporous magnesium carbonate include pharmaceutical ones such as drug stabilizer [7,8] and anticoagulant [9]. Additionally, a mesoporous structure could make these materials suitable as adsorbents for pollutants and other substances. An interesting example of this is a report on mesoporous magnesium carbonate, synthesized with methanol, and treated with additives, which showed good adsorption of $CO_2$, due to the high surface area (over 500 $m^2/g$), with the inorganic additives increasing $CO_2$ uptake and selectivity [10].

Another potential use of high surface area carbonates is the adsorption of contaminants. Shahwan et al. report that $MgCO_3$ is a better adsorbent of $Pb^{2+}$ and $Zn^{2+}$ ions than clay minerals [11]. Mesoporous calcium carbonates have also been reported as good adsorbents for heavy metal ions ($Pb^{2+}$ and $Cd^{2+}$); the removal efficiency depended on the crystal structure [12]. Shan et al. showed that synthetic nesquehonite is a highly efficient agent for removing $Cu^{2+}$, which was precipitated as a mixture of hydroxides and carbonates [13]. A novel application of hydromagnesite is in the directional displacement of fluids in porous media [14].

This shows the importance of studying the synthesis of magnesium carbonates. Many of the synthesis methods for magnesium carbonate, including those using supercritical carbon dioxide ($scCO_2$), with ethanol as a cosolvent [15] and mineral carbonation in aqueous solution [16] usually do not yield mesoporous materials (pores of 2–50 nm). Another option for cosolvent is methanol, which can increase the solvation power of the main solvent, to control the morphology of carbonates and has been used as a control factor of the pore size according to traditional synthesis works but can result in amorphous carbonates [17]. Reaction temperature is also an important factor that affects pore size [6,7]. However, organic solvents can contribute to emission of pollutants [18].

There are some examples of works exploring mineral carbonation with magnesium, such as that of Yoo et al. [19] in which magnesium comes from seawater desalination waste and is precipitated as carbonates using alkanolamines.

In CCS, $CO_2$ is usually delivered and transported in supercritical state for geological storage [20]. Therefore, it is important to study mineral carbonation by reaction with $scCO_2$, which is by itself a solvent as well as a reactant, therefore, these reactions may not require the use of organic solvents such as methanol and ethanol, making it a greener method.

Here we compare $scCO_2$ and aqueous synthesis methods with the objective of producing mesoporous magnesium carbonates, via environmentally friendly methods.

## 2. Materials and Methods

Aqueous synthesis by $CO_2$ sequestration was based on the method of de Vito et al. [16]. We bubbled $CO_2$ through a Pasteur pipette into magnesium solutions in deionized water in a stoppered flask, with a flow rate equivalent to 1.1 g/min (Figure 1a).
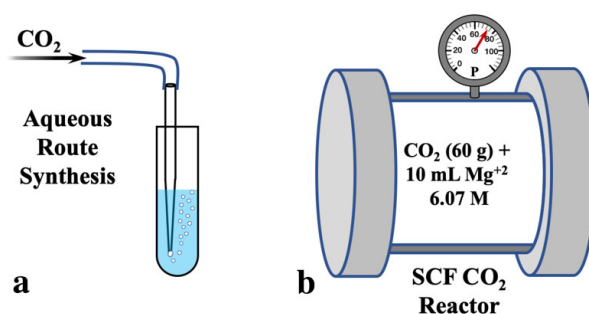


**Figure 1.** Schematic diagrams showing the experimental method for aqueous synthesis, (**a**) bubbling $CO_2$ gas, and (**b**) supercritical fluid (SCF) closed reactor (kept at constant temperature in a hot water bath, not shown for clarity).

Three precursors salts (all reactive grade, CTR Scientific, Monterrey, México) were used for both routes: $MgCl_2 \cdot 6H_2O$ (10 mL, 6.07 M), $Mg(NO_3)_2 \cdot 6H_2O$ (10 mL, 6.07 M), $MgSO_4 \cdot 7H_2O$ (20 mL, 3.036 M). The pH was adjusted to 8–9 with $NH_4OH$ and reactions were carried out for 25 and 60 min at 5, 21, and 70 °C, as shown in Table 1.

**Table 1.** Design of experiments.

| Experimental Method | Precursors Salts | Reaction Time | Reaction Temperature | Drying Temperature |
|---|---|---|---|---|
| Aqueous Synthesis | $MgCl_2 \cdot 6H_2O$ | 25 and 60 min | 5, 21, and 70 °C | 40 °C |
| | $Mg(NO_3)_2 \cdot 6H_2O$ | | | |
| | $MgSO_4 \cdot 7H_2O$ | | | |
| scCO₂ Synthesis | $Mg(NO_3)_2 \cdot 6H_2O$ | 12 h | 35–40 °C | 40 °C |
| | | | | 100 °C |

In the supercritical synthesis, we added 60 g of $CO_2$ (enough to reach a pressure >74 bar) in a custom-made reactor, with a volume of 240 mL (Figure 1b), containing 10 mL of 6.07 M $Mg(NO_3)_2 \cdot 6H_2O$ (pH adjusted to 8–9 with $NH_4OH$). The reactor was hermetically closed and placed in a water bath at 35–40 °C to reach and maintain supercritical conditions, monitored by observation of the phase change through a window. After 12 h of reaction, the reactor was depressurized. Solid products were collected and washed five times with 5 mL of distilled water, then oven-dried for 12 h at 100 °C (scCO₂-od). To analyze the effect of the drying temperature on the material structure, the same synthesis procedure was carried out, and the sample was dried over a hot plate at 40 °C for 12 h (scCO₂-hpd).

Morphology was observed with a Zeiss EVO MA scanning electron microscope (SEM), from Carl Zeiss AG (Oberkoche, Germany). Some samples were sputter coated with 5 nm of Au, to prevent charging.

Diffraction patterns of selected products were obtained with a Siemens/Bruker D5000 diffractometer from Bruker AXS (Karlsruhe, Germany), using Cu $K_\alpha$ radiation ($\lambda$ = 1.54184 Å), 2θ angle from 5° to 70° with a scan rate of 5 °/min. Profex, an open source program by Nicola Döbelin (www.profex-xrd.org), was used for Rietveld refinement. Raman spectroscopy for the samples scCO₂-od and aqueous route was performed in an OceanOptics (Orlando, FL, USA) QE65000 equipment (785.0 nm laser, 5 s acquisition time). Raman spectroscopy for the scCO₂-hpd samples was performed in a Jasco NRS-5100 equipment (785.0 nm laser, 60 s acquisition time), from JASCO Corporation (Hachioji, Japan). BET analysis was performed in a Quantachrome Autosorb iQ®, from Anton Paar Instrumentsn (Boynton Beach, FL, USA), in a 6 mm cell, samples were previously degassed for 2 h at 80 °C followed by 10 h at 100 °C.

For comparison, another magnesium carbonate sample was prepared by aqueous route by reaction of magnesium chloride, $MgCl_2 \cdot 6H_2O$ [Productos Químicos Monterrey S.A. de C.V., Monterrey, México, ACS grade], with potassium hydroxide [KOH, Productos Químicos Monterrey S.A. de C.V., ACS grade] and sodium bicarbonate [$NaHCO_3$, CTR Scientific, Monterrey, México, ACS grade], by dissolving 0.1 mole of each in 100 mL of water.

A commercial magnesium carbonate (Gym Chalk, Gibson Gym Chalk, Gibson Athletic, Denver, CO, USA, purchased at Amazon.com) was also characterized by XRD and BET for comparison.

## 3. Results

The net chemical reaction for the synthesis of magnesium carbonate is shown in Equations (1) and (2): a $Mg^{2+}$ precursor (MgX, X represents the anion) reacts in an alkaline

medium to form $Mg(OH)_2$, followed by a carbonation reaction producing $MgCO_3$. At the lowest temperature (5 °C), due to slow kinetics, no precipitate was formed.

$$MgX + 2OH^-(aq.) \rightarrow Mg(OH)_2 \tag{1}$$

$$Mg(OH)_2 + HCO_3^-(aq.) \rightarrow MgCO_3 + H_2O + OH^-(aq.) \tag{2}$$

Different $MgCO_3$ structures were obtained, including hydromagnesite ($Mg_5(CO_3)_4(OH)_2 \cdot 4H_2O$), dypingite ($Mg_5(CO_3)_4(OH)_2 \cdot 5H_2O$), lansfordite ($MgCO_3 \cdot 5H_2O$), magnesite ($MgCO_3$), and nesquehonite ($MgCO_3 \cdot 3H_2O$) according to XRD analysis. The density of these hydrated magnesium carbonates depends on their structure, hydromagnesite usually is 2–2.5 times denser than dypingite [3], therefore, it would present less specific surface area.

For the reaction with $Mg(NO_3)_2 \cdot 6H_2O$ as precursor at 70 °C, spherical nanoparticles were observed (Figure 2a), these are hydromagnesite according to XRD results (shown below). Unluer et al. [3] have reported similar hydromagnesite spherical structures. The carbonate yields at 70 °C were higher than at 21 °C, which is expected, since the solubility of $CO_2$ decreases at higher temperatures, and the formation of hydromagnesite is not thermodynamically favorable below 55 °C [21].
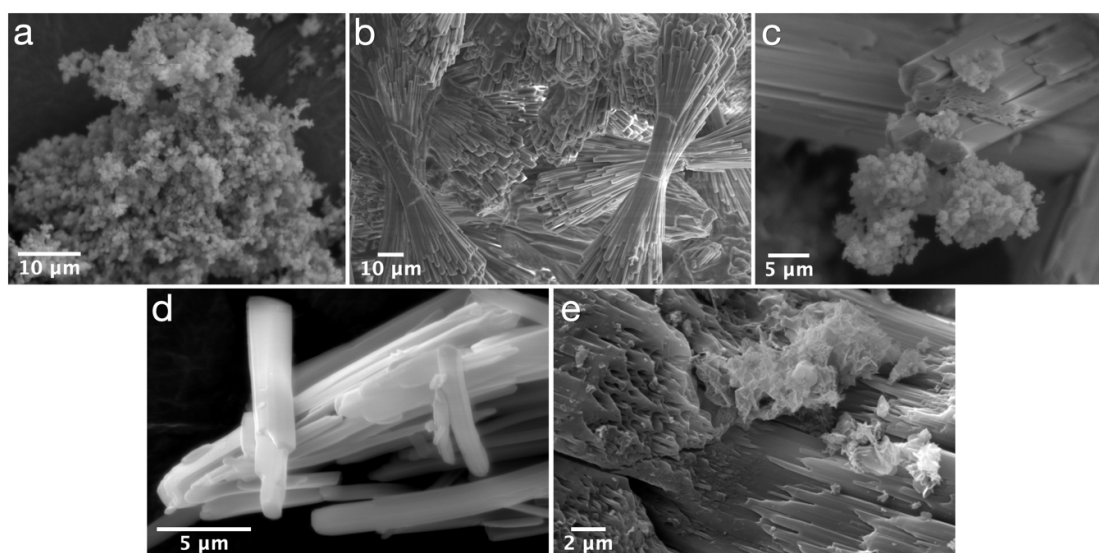


**Figure 2.** Scanning electron micrographs of carbonate products (acquired in variable pressure mode), showing representative morphologies from aqueous syntheses (**a**–**c**), from scCO₂-od (**d**) scCO₂-hpd (**e**).

With $MgSO_4$ as precursor (25 min reaction, 21 °C), we obtained a product with a morphology of rods of ca. 20 μm, conjoined and extending from a compact center (Figure 2b). This morphology is usually known as dumbbell-shaped aggregates (DSA) [22]. This type of morphology can appear as an intermediate state of spherulitic growth of many minerals. However, we should remark that in our material we did not observe spherulitic crystals, which may indicate that this nonequilibrium morphology could have been favored under our synthesis conditions. One way this might have happened is by the appearance of a large number of nuclei at the beginning, which then grow and deplete precursors before crystals can achieve the spherulitic morphology.

Using magnesium chloride and nitrate as precursors, at the same reaction temperature, we obtained products with two different morphologies (Figure 2c), containing magnesium hydroxide [23] in addition to the carbonate. The synthesis with scCO₂ generated acicular crystals exclusively, ca 10 μm long (Figure 2d). Our results show that carbonate crystal sizes changed with synthesis temperature, in a matter consistent with the reported trend [23] that smaller crystals are favored at higher temperature. Additionally, the drying process

applied to the samples influenced the surface appearance, given that the sample dried over a hot plate has a rougher surface (Figure 2e). Considering the morphology observed by SEM, the DSA product and the supercritical products were characterized further.

The diffractogram of the scCO$_2$-od carbonate product (Figure 3a) matches the diffraction pattern of nesquehonite, (MgCO$_3$·3H$_2$O). These crystals look similar to those found by Hänchen et al. [24] using CO$_2$ at a pressure of 1 bar, using sodium carbonate as the base, and CO$_2$ at temperatures and pressures above the critical point (120 °C, 100 bar) but they found precipitation of hydromagnesite and magnesite exclusively. The latter was favored by longer reaction times. By contrast, Yoo et al. found mostly nesquehonite when using supercritical CO$_2$ at moderate temperatures ($\leq$60 °C), and when using short chain alkanolamines as the base, with hydromagnesite favored at higher temperatures (70 °C) [19].
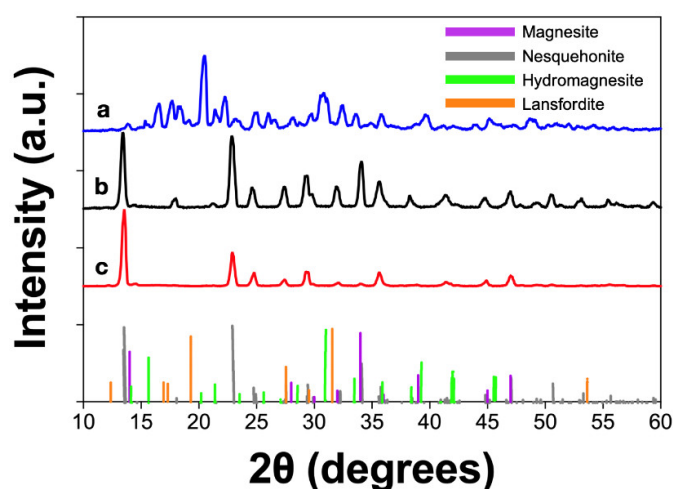


**Figure 3.** X-ray diffraction patterns of (**a**) DSA (dumbbell-shaped aggregates) product, (**b**) magnesium carbonate, from supercritical synthesis, hot plate dried, scCO$_2$-hpd, and (**c**) magnesium carbonate from supercritical synthesis, oven dried, scCO$_2$-od. Reference peaks of crystalline structures with the highest correlation are shown as determined by Rietveld refinement.

XRD of commercial carbonate showed that it was hydromagnesite, which is typically the more stable hydrated phase of magnesium carbonate [25].

The diffractogram of the DSA material (Figure 3b) corresponds to a mixture of crystalline structures. Rietveld refinement was used to correlate those peaks to four structures: magnesite (MgCO$_3$), nesquehonite (MgCO$_3$·3H$_2$O), hydromagnesite (Mg$_5$(CO$_3$)$_4$(OH)$_2$·4H$_2$O), and lansfordite (MgCO$_3$·5H$_2$O), with a good match found only for the last three. For the carbonate obtained with the MgSO$_4$·7H$_2$O precursor, the DSA morphology with elongated crystals was favored over regular spherulitic growth as previously reported [3].

The diffractogram of the scCO$_2$ carbonate product with hot plate drying (Figure 3c) shows a mixture of crystalline structures of hydrated magnesium carbonate. According to the Rietveld refinement the identified structures correspond to magnesite, hydromagnesite, nesquehonite, and lansfordite.

The proportion of each of the phases is shown in Table 2. The difference between the composition of both scCO$_2$ products was expected since magnesium carbonate is sensitive to temperature and dehydrates when heated at moderately high temperatures [3]. The scCO$_2$-hpd product contains a higher percentage of a more hydrated phase, lansfordite and hydromagnesite, compared with the scCO$_2$-od for which the main component is nesquehonite.

**Table 2.** Magnesium carbonates phase composition determined by Rietveld refinement for products from scCO$_2$ synthesis (oven dried and hot plate dried), and dumbbell-shaped structures from aqueous synthesis.

| Phase | scCO$_2$-od | scCO$_2$-hpd | DSA |
|---|---|---|---|
| Magnesite | 0% | 20% | 0% |
| Nesquehonite | 65% | 0% | 54% |
| Lansfordite | 27% | 60% | 40% |
| Hydromagnesite | 8% | 20% | 6% |

The structures of the carbonates produced by the aqueous route changed depending on the precursor. For nitrate, the dried product showed a mixture of dypingite and hydromagnesite (Figure 4a). With sulfate as precursor, in samples that did not show the DSA morphology, the peaks correspond to a mixture of nesquehonite and hydromagnesite (Figure 4b), without peaks for magnesium sulfates. We note that since we dried these products at relatively high temperatures there may have been partial dehydration of the precipitate.
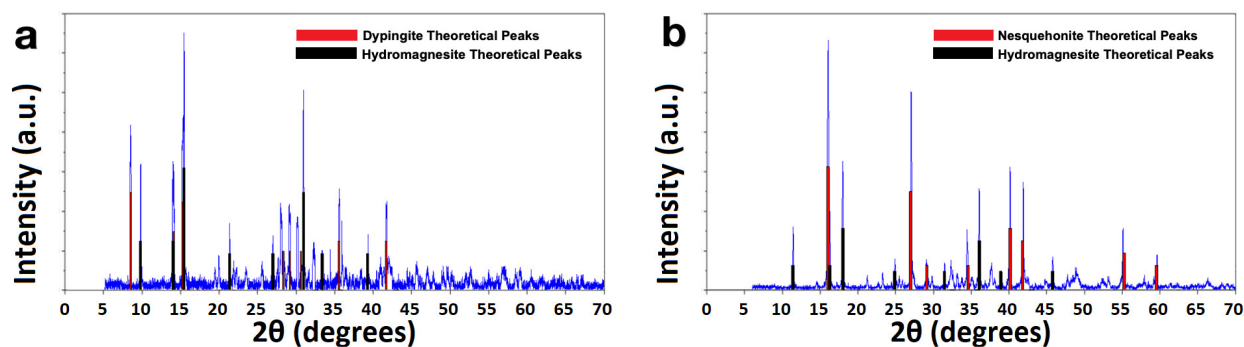


**Figure 4.** X-ray diffraction patterns (blue lines) of (**a**) magnesium carbonate, from aqueous route synthesis with nitrate as precursor, showing a mixture of dypingite and hydromagnesite, according to Rietveld refinement. (**b**) Magnesium carbonate, from aqueous route synthesis with sulfate as precursor, showing a mixture of nesquehonite and hydromagnesite, according to Rietveld refinement.

Raman spectra of the DSA product and scCO$_2$-od nesquehonite (Figure 5) show peaks characteristic of the carbonate ion (CO$_3^{2-}$) at 1107 and 1400–1500 cm$^{-1}$ [26]. For the DSA product, the wide Raman peak at 1014 cm$^{-1}$ indicates that it is formed by a mixture of sulfate and carbonate. Magnesium sulfates present Raman peaks that depend on the degree of hydration, going from a peak at 983.6 cm$^{-1}$, for hexahydrite, and changing to higher wavenumbers as the degree of hydration decreases, up to 1046.1 cm$^{-1}$ for the monohydrate (kieserite, MgSO$_4$·H$_2$O) [27]. The observed peak is centered between those corresponding to the tetrahydrate (MgSO$_4$·4H$_2$O, Starkeyite, 1000.3 cm$^{-1}$) and the trihydrate (1023.8 cm$^{-1}$), suggesting that these two components are present in the DSA product, in addition to hexahydrate. The sulfate does not show in the corresponding diffractogram (Figure 3) but we suspect that low intensity sulfate peaks may be among the several broad peaks observed.
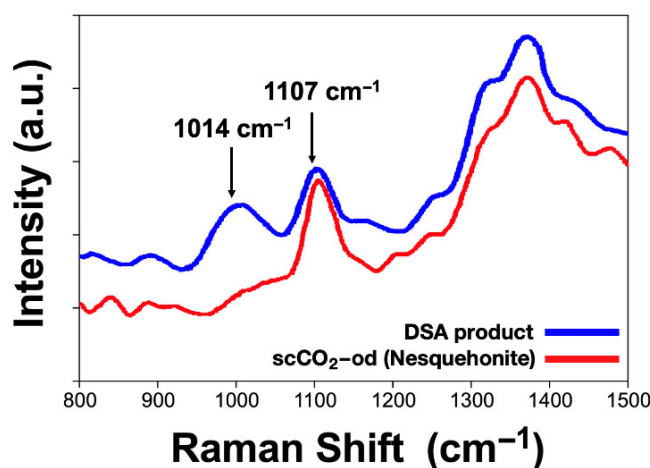
**Figure 5.** Raman spectra of the DSA product (aqueous route, blue curve, above) and $scCO_2$-od (nesquehonite, supercritical route, red curve), acquired with a 785 nm laser, 5 s acquisition time.

For comparison, Figure 6 shows the Raman spectrum of the $scCO_2$-hpd material, which only shows the characteristic peak of the symmetric stretching of the carbonate ion at 1100 cm$^{-1}$ [26].
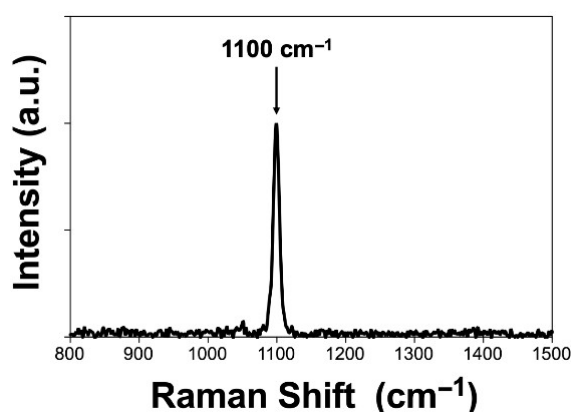


**Figure 6.** Raman spectrum of the $scCO_2$-hpd, acquired with a 785 nm laser, 60 s acquisition time.

BET isotherms (measured with adsorption of $N_2$ at 77.35 K) are shown in Figure 7a, these results show specific surface areas of 39.1 m$^2$g$^{-1}$ for the DSA product, 70.4 m$^2$g$^{-1}$ for the $scCO_2$-od nesquehonite product, and a lower value of 19.8m$^2$g$^{-1}$ for the $scCO_2$-hpd product. The average pore sizes were 1.02 nm for nesquehonite, 3.78 nm for the DSA product, and 5.48 nm for the $scCO_2$ product dried on a hot plate, according to density functional theory (DFT) modeling (Figure 7b,c) and in both cases the pore size distribution is relatively wide. These results are better than the surface area of carbonate made by reaction with bicarbonate, and that of commercial carbonate, as shown in Table 3. According to the IUPAC classification of adsorption isotherms [28,29], the $scCO_2$ -hpd carbonate isotherm shows an H3 behavior which is characterized by slit-shaped pores, additionally it behaves as type IV isotherm which corresponds to a micro-mesoporous material with an average pore size of 5.48 nm. We should warn the reader that the heat treatment at 80 °C prior to BET measurements may have altered the hydration state of the carbonates, however this is a necessary step to ensure complete degassing, which otherwise would give inaccurate readings. By using the same pretreatment for the oven-dried and hot-plate dried materials we aimed to make both sets of results comparable.
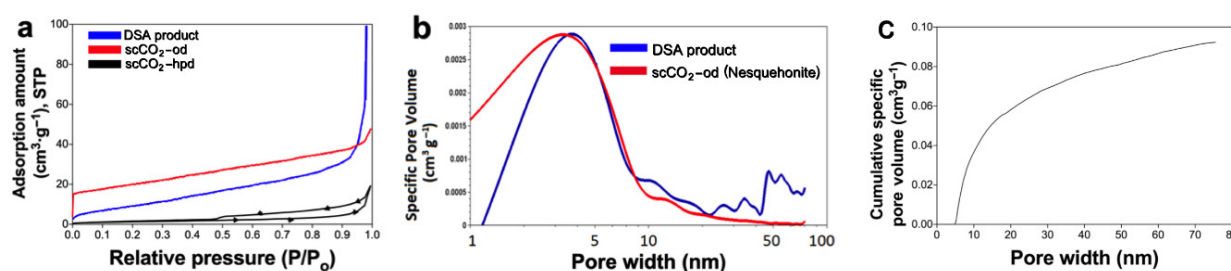
**Figure 7.** (**a**) BET adsorption isotherms (adsorbed amount cm$^3$ g$^{-1}$ vs. relative pressure) of the DSA product, scCO$_2$-hpd, and scCO$_2$-od. (**b**) Pore volume cm$^3$ g$^{-1}$ vs. pore width (nm) of DSA and nesquehonite product (scCO$_2$-od) calculated by density functional theory (DFT). The apparent pores of $\approx$50 μm are considered a result of experimental noise, since no pores of these sizes were observed in the SEM (**c**) Cumulative specific pore volume cm$^3$g$^{-1}$ vs. pore width (nm) of the scCO$_2$-hpd product.

**Table 3.** Specific surface areas and average pore sizes for different magnesium carbonates.

| Sample | Specific Surface Area (m$^2$g$^{-1}$) | Average Pore Size (nm) |
|---|---|---|
| scCO$_2$-od nesquehonite | 70.4 | 1.02 |
| DSA | 39.1 | 3.78 |
| MgCl$_2$ + NaHCO$_3$ + KOH | 11.8 | 50 |
| Commercial carbonate | 18.1 | 4.89 |
| scCO$_2$ -hpd | 19.8 | 5.48 |

We should note that nesquehonite has been reported to form in a matter of minutes [30], suggesting that our supercritical synthesis route may not require reaction times as long as 12 h, and we intend to explore what is the shortest time for full precipitation.

## 4. Conclusions

We presented two synthesis methods for mesoporous magnesium carbonates from CO$_2$ that avoid the use of organic cosolvents, which may be useful in green synthesis routes. Moreover, the capture of CO$_2$ achieved through these routes may potentially contribute to reduce atmospheric CO$_2$ concentration by mineralization. We used solid CO$_2$ for convenience, but supercritical conditions also could be reached by syphoning liquid CO$_2$ into the reactor, which should not change the results and would be more environmentally friendly.

Due to the relatively high surface area and small pore sizes of these materials, we expect that they may be useful as adsorbents and in other applications, including capillary transport and in pharmaceutical and drug delivery applications, if their surface area could be increased further by fine tuning the synthesis parameters.

We found conditions for aqueous synthesis that allow isolating the morphology called dumbbell shaped aggregates which showed a large specific surface area and mesopores according to BET measurements. These crystals appear to be an intermediate step of growth of spherulitic crystals and were formed by a combination of carbonate and sulfate according to XRD and Raman characterization.

Carbonate synthesized in supercritical CO$_2$ and oven dried had a larger specific surface area and smaller pores than the DSA material. This material had a nesquehonite crystal structure, according to XRD, and was composed solely of magnesium carbonate. Carbonates synthesized in scCO$_2$ and hot plate dried resulted in a micro-mesoporous material with a smaller surface area. Both carbonates synthesized in scCO$_2$ had a larger area compared with commercial magnesium carbonate and they provide a simple synthesis method that could be implemented in existing CCS facilities during the process where the CO$_2$ is compressed to obtain scCO$_2$ for transportation to geological storage.

## References

1. National Academies of Sciences, Engineering, and Medicine. *Negative Emissions Technologies and Reliable Sequestration: A Research Agenda*; The National Academies Press: Washington, DC, USA, 2019. [CrossRef]
2. Sanna, A.; Uibu, M.; Caramanna, G.; Kuusik, R.; Maroto-Valer, M.M. A review of mineral carbonation technologies to sequester $CO_2$. *Chem. Soc. Rev.* **2014**, *43*, 8049–8080. [PubMed]
3. Unluer, C.; Al-Tabbaa, A. Characterization of Light and Heavy Hydrated Magnesium Carbonates Using Thermal Analysis. *J. Therm. Anal. Calorim.* **2014**, *115*, 595–607.
4. Farhang, F.; Oliver, T.K.; Rayson, M.; Brent, G.; Stockenhuber, M.; Kennedy, E. Experimental study on the precipitation of magnesite from thermally activated serpentine for $CO_2$ sequestration. *Chem. Eng. J.* **2016**, *303*, 439–449.
5. Glasser, F.P.; Jauffret, G.; Morrison, J.; Galvez-Martos, J.-L.; Patterson, N.; Imbabi, M.S.-E. Sequestering $CO_2$ by Mineralization into Useful Nesquehonite-Based Products. *Front. Energy Res.* **2013**, *4*, 3.
6. Frykstrand, S.; Forsgren, J.; Mihranyan, A.; Strømme, M. On the pore forming mechanism of Upsalite, a micro- and mesoporous magnesium carbonate. *Microporous Mesoporous Mater.* **2014**, *190*, 99–104.
7. Yang, J.; Alvebratt, C.; Lu, X.; Bergström, C.A.S.; Strömme, M.; Welch, K. Amorphous magnesium carbonate nanoparticles with strong stabilizing capability for amorphous ibuprofen. *Int. J. Pharm.* **2018**, *548*, 515–521.
8. Cheung, O.; Zhang, P.; Frykstrand, S.; Zheng, H.; Yang, T.; Sommariva, M.; Zou, X.; Strömme, M. Nanostructure and pore size control of template-free synthesised mesoporous magnesium carbonate. *RSC Adv.* **2016**, *6*, 74241–74249.
9. Frykstrand, S.; Forsgren, J.; Cheung, O.; Zhang, P.; Hong, J.; Strømme, M.; Ferraz, N. Study of mesoporous magnesium carbonate in contact with whole human blood. *RSC Adv.* **2016**, *6*, 52810–52816.
10. Vall, M.; Hultberg, J.; Strömme, M.; Cheung, O. Carbon dioxide adsorption on mesoporous magnesium carbonate. *Energy Procedia* **2019**, *158*, 4671–4676.
11. Shahwan, T.; Zünbül, B.; Eroğlu, A.E.; Yılmaz, S. Effect of magnesium carbonate on the uptake of aqueous zinc and lead ions by natural kaolinite and clinoptilolite. *Appl. Clay Sci.* **2005**, *30*, 209–218.
12. Wang, P.; Shen, T.; Li, X.; Tang, Y.; Li, Y. Magnetic Mesoporous Calcium Carbonate-Based Nanocomposites for the Removal of Toxic Pb(II) and Cd(II) Ions from Water. *ACS Appl. Nano Mater.* **2020**, *3*, 1272–1281.
13. Shan, Q.; Zhang, Y.; Xue, X. Removal of copper from wastewater by using the synthetic nesquehonite. *Environ. Prog. Sustain. Energy* **2013**, *3*, 543–546.
14. Castilleja-Escobedo, O.; Sánchez-García, R.E.; Nigama, K.D.P.; López-Salinas, J.L. Directional displacement of non-aqueous fluids through spontaneous aqueous imbibition in porous structures. *Chem. Eng. Sci.* **2020**, *228*, 115959.

15. Kim, K.D.; Kim, Y.D.; Kim, S.W. Synthesis of Porous Magnesium Oxide Cubes with Nano-Grain Structure in Supercritical $CO_2$/Ethanol Solution. *J. Nanosci. Nanotechnol.* **2002**, *11*, 5723–5728.

16. de Vito, C.; Ferrini, V.; Mignardi, S.; Cagnetti, M.; Leccese, F. Progress in carbon dioxide sequestration via carbonation of aqueous saline wastes. *Period. Mineral.* **2012**, *81*, 333–344.

17. Nakashima, Y.; Takai, C.; Razavi-Khosroshahi, H.; Suthabanditpong, W.; Fuji, M. Synthesis of ultra-small hollow silica nanoparticles using the prepared amorphous calcium carbonate in one-pot process. *Adv. Powder Technol.* **2018**, *29*, 904–908.

18. DeSimone, J.M. Practical Approaches to Green Solvents. *Science* **2002**, *297*, 799–803.

19. Yoo, Y.; Kang, D.; Choi, E.; Park, J.; Hugh, I. Morphology control of magnesium carbonate for $CO_2$ utilization using $Mg^{2+}$ ions in industrial wastewater depending on length of alkyl chain of primary alkanolamine, reaction temperature, $CO_2$ concentration, and $Mg^{2+}/Na^+$ ratio. *Chem. Eng. J.* **2019**, *370*, 237–250.

20. Sim, S.; Cole, I.S.; Choi, Y.S.; Birbilis, N. A review of the protection strategies against internal corrosion for the safe transport of supercritical $CO_2$ via steel pipelines for CCS purposes. *Int. J. Greenh. Gas Control* **2014**, *29*, 185–199.

21. Langmuir, D. Stability of Carbonates in the system $MgO$-$CO_2$-$H_2O$. *J. Geol.* **2015**, *73*, 730–754.

22. Perry, C.T.; Salter, M.A.; Harborne, A.R.; Crowley, S.F.; Jelks, H.L.; Wilson, R.W. Fish as major carbonate mud producers and missing components of the tropical carbonate factory. *Proc. Natl. Acad. Sci. USA* **2011**, *108*, 3865–3869. [CrossRef] [PubMed]

23. Ding, W.; Ouyang, J.; Yang, H. Synthesis and characterization of nesquehonite ($MgCO_3·3H_2O$) powders from natural talc. *Powder Technol.* **2016**, *292*, 169–175. [CrossRef]

24. Hänchen, M.; Prigiobbe, V.; Baciocchi, R.; Mazzotti, M. Precipitation in the Mg-carbonate system—effects of temperature and $CO_2$ pressure. *Chem. Eng. Sci.* **2008**, *63*, 1012–1028. [CrossRef]

25. Botha, A. DTA and FT-IR analysis of the rehydration of basic magnesium carbonate. *J. Therm. Anal. Calorim.* **2003**, *71*, 987–996. [CrossRef]

26. Forsgren, J.; Frykstrand, S.; Grandfield, K.; Mihranyan, A.; Strömme, M. A Template-Free, Ultra-Adsorbing, High Surface Area Carbonate Nanostructure. *PLoS ONE* **2013**, *8*, e68486. [CrossRef] [PubMed]

27. Wang, A.; Freeman, J.J.; Jolliff, B.L.; Chou, I. Sulfates on Mars: A systematic Raman spectroscopic study of hydration states of magnesium sulfates. *Geochim. Cosmochim. Acta* **2006**, *70*, 6118–6135. [CrossRef]

28. Alothman, Z.A. A review: Fundamental aspects of silicate mesoporous materials. *Materials (Basel)* **2012**, *5*, 2874–2902. [CrossRef]

29. Sing, K.S.; Everett, D.H.; Haul, R.A.W.; Moscou, L.; Pierotti, R.A.; Rouquerol, J.; Siemieniewska, T. Reporting Physisorption Data for Gas/Solid Systems with Special Reference to the Determination of Surface Area and Porosity. *Pure Appl. Chem.* **1985**, *57*, 603–619. [CrossRef]

30. Ferrini, V.; de Vito, C.; Mignardi, S. Synthesis of nesquehonite by reaction of gaseous $CO_2$ with Mg chloride solution: Its potential role in the sequestration of carbon dioxide. *J. Hazard. Mater.* **2009**, *168*, 832–837. [CrossRef]